

Optimal Particle-Conserved Linear Encoding for Practical Fermionic Simulation

M. H. Cheng,^{1,2,*} Yu-Cheng Chen,^{3,4,*} Qian Wang,³ V. Bartsch,² M. S. Kim,^{1,†} Alice Hu,^{3,5,‡} and Min-Hsiu Hsieh^{4,§}

¹*Department of Physics Blackett Laboratory, Imperial College London, SW7 2AZ, United Kingdom*

²*Fraunhofer Institute for Industrial Mathematics, Fraunhofer-Platz 1, 67663 Kaiserslautern, Germany*

³*Department of Mechanical Engineering, City University of Hong Kong, Kowloon, Hong Kong SAR 999077, China*

⁴*Hon Hai (Foxconn) Research Institute, Taipei, Taiwan*

⁵*Department of Materials Science and Engineering, City University of Hong Kong, Kowloon, Hong Kong SAR 999077, China*

Particle-conserved subspace encoding reduces resources for quantum simulations, but a scalable and resource-minimal protocol for M modes and N particles, $\mathcal{O}(N \log M)$ qubits and $\mathcal{O}(\text{Poly}(M))$ measurements bases, has remained unknown. We demonstrate optimal encoding with classical parity check code generated by the Randomized Linear Encoder and propose the Fermionic Expectation Decoder for scalable probability decoding in $\mathcal{O}(M^4)$ bases. The protocol is tested with variational quantum eigensolver on LiH in the STO-3G and 6-31G basis, and H₂ potential energy curve in the 6-311G* basis.

Introduction.—Simulating many-body fermionic systems is an essential tool in various fields like quantum chemistry, condensed matter, and high energy physics [1–3], promising better designs for batteries and drugs, new quantum technologies, and discoveries in the exotic nature of reality [4–6]. However, accurate fermionic simulation on classical computers requires exponential computational resources [7]. While a quantum computer is expected to overcome this limit, it remains a central challenge to demonstrate quantum advantages in this domain.

Electronic structure Hamiltonian encoding maps fermionic operators from the Fock space to qubit operators in the qubit space. The standard approaches such as the Jordan-Wigner, Parity, and Bravyi-Kitaev transformations [8, 14] encode M fermionic modes to M qubits, regardless of the number of electrons N . However, since all fermionic Hamiltonians must conserve fermions, interesting physics depends only on the particle conserved subspace and takes only $[N \log M]$ qubits to encode in the precision limit $M \gg N$ [15, 16]. Logarithmic scaling in M enormously relieves the qubit resource requirements for simulation in the high precision limit, and it could serve as a powerful tool in the practical implementation of quantum simulation on near-term and fault-tolerant devices [17].

Another important aspect of fermionic encoding is the measurement scalability of the two-electron reduced density matrix (2-RDM). Unlike classical encoding, quantum encoding changes the measurement complexity in two ways. First, non-linear methods such as the projector approach [18] and the Qubit Efficient Encoding (QEE) [12] have attained the $[N \log M]$ qubit scaling via a di-

rect fermionic state to qubit state encoding. However, it is plagued with unscalable encoding and measurement basis preparation cost of $\mathcal{O}(M^N)$, limiting its applications to fermionic systems with few electrons. Secondly, suppose a specific grouping is found to mitigate the basis preparation cost. The resulting grouping will still suffer from an unbounded number of commuting Pauli strings.

Linear compression resolves the measurement and decoding cost. All linear compression methods, such as the segment code [9] and graph-based encoding [10], exhibit polynomial measurement costs with respect to M . However, they fail to efficiently encode fermionic modes and large number of electrons. The current best linear encoding demonstrates poly-logarithmic $\mathcal{O}(N^2(\log M)^4)$ qubit scaling [11] that overcomes the scaling in the previous works, but quadratic in N and quartic in $\log M$ limits its applicability only to molecules that require a large basis set not accessible to near-term devices. The optimal compression rate in linear compression remains unknown.

In this Letter, we propose a scalable encoder-decoder protocol with optimal qubit to measurement trade-off. Using parity check code of error correction code (CEC) that obeys the Gilbert-Varshamov (GV) bound [10, 19, 20], we prove that optimal linear encoder has a qubit resource upper bound of $2N \log M$. We propose the Fermionic Observables Decoding (FED) algorithm which incorporates a classical decoder to decode fermionic probability distribution of a linearly encoded Hilbert space to the unencoded space. FED is applicable for arbitrary linear encoding. By avoiding calculation in the encoded space, FED allows polynomial time classical post-processing using a classical decoder. The scalability of our protocol depends on whether a CEC encoder-decoder protocol that obeys the GV bound can be efficiently solved. Indeed, polynomial time encoder and decoder can be found in examples such as the geometric Goppa code [21, 22] and Gallager’s LDPC code [23, 24]. Our protocol completely resolves scalability issue in non-linear encodings in both the encoding-decoding process

* These authors contributed equally to this work

† m.kim@imperial.ac.uk

‡ alicehu@cityu.edu.hk

§ min-hsiu.hsieh@foxconn.com

	Jordan Wigner [8]	Segment [9]	Graph-Based [10]	Polylog [11]	QEE [12]	Our Work
Qubit cost	M	$M - \frac{M}{2N}$	$M - \frac{M}{N}$	$O(N^2(\log M)^4)$	$[N \log M]$	$[2N \log M]$
Measurements	$O(M^3)$ [13]	$O(M^4)$	$O(M^4)$	$O(M^4)$	$O(M^N)$	$O(M^4)$

TABLE I. This table compares the qubit-to-measurement trade-off of the existing encoding schemes at the regime $M \gg N$. The measurement cost is computed under our fermionic operator decoding framework.

via parity check code, scalable measurement bases and novel embedding of parity check decoder in fermionic observable post-processing. Our result finds application for encoding large fermionic systems and NISQ or fault-tolerant quantum algorithms such as quantum signal processing [25].

To demonstrate the optimal encoder-decoder protocol, we introduce the randomized linear encoder (RLE) algorithm with a look-up table classical decoder useful for encoding large-mode problems with a bounded number of electrons. RLE encoded circuits adheres to the $2N \log M$ qubit bound, surpassing the qubit compression rates of the segment code and graph-based encoding for all N and M . We test the protocol using the variational quantum eigensolver (VQE) on LiH in the STO-3G and 6-31G basis at a bond length of 2.5 Å with the hardware-efficient ansatz (HEA) [26, 27], and H₂ in the 6-311G* basis. The optimally encoded LiH noiseless simulation achieves chemical accuracy using 30 CNOT gates with 5 layers, compared to the JW encoded version which does not converge even after 6 layers. We also compare both cases with the IBM Sherbrooke noise model. We report that the H₂ simulation achieves chemical accuracy across all bond lengths using only 66 local CNOT gates.

General Framework—Given a second-quantized electronic structure Hamiltonian:

$$\hat{H} = \sum_{ij} h_{ij} \hat{a}_i^\dagger \hat{a}_j + \sum_{ijkl} g_{ijkl} \hat{a}_i^\dagger \hat{a}_j^\dagger \hat{a}_k \hat{a}_l, \quad (1)$$

qubit operator representation of the excitation operators $\hat{a}_i^\dagger \hat{a}_j$ and $\hat{a}_i^\dagger \hat{a}_j^\dagger \hat{a}_k \hat{a}_l$, collectively denoted as \hat{O} , determines qubit, gate, and measurement complexities of quantum simulation. By reviewing the general framework of fermionic-to-qubit mapping, we reveal the connection between qubit operator and parity check code complexity, and encoding-decoding protocol with optimal qubit-to-measurement trade-off is proposed.

In linear code, bitstrings with fixed hamming weight, corresponding to number conserved states, can be encoded via a binary matrix map $\mathbf{G} : \mathbb{F}_2^M \rightarrow \mathbb{F}_2^Q$. Such matrix map is connected to the encoding of \hat{O} via three binary vectors $\vec{a}, \vec{b}, \vec{c} \in \mathbb{F}_2^M$; such that $\vec{b} \in S_{\hat{O}} = \{\vec{b} | H(\vec{b}) = N, \hat{O}|\vec{b}\rangle \neq |\vec{b}\rangle\}$, \vec{a} induces state transitions via bitwise addition $\vec{a} \oplus \vec{b}$, and \vec{c} computes the parity information of \vec{b} via $\vec{c} \cdot \vec{b}$. They are directly connected to qubit operators:

$$X^{\vec{a}} = \prod_{m=1}^M \sigma_{x,m}^{\vec{a}[m]}, P^{\vec{b}} = \prod_{m=1}^M \frac{1 + (-1)^{\vec{b}[m]} \sigma_{z,m}}{2}, Z^{\vec{c}} = \prod_{m=1}^M \sigma_{z,m}^{\vec{c}[m]}, \quad (2)$$

dubbed as the X-string, Z-string, and P-string. Given an $M \times M$ encoder, such as the BK encoding [14], the operators are encoded as [9]:

$$\mathcal{E}(X^{\vec{a}}) = X^{\mathbf{G}\vec{a}}, \mathcal{E}(P^{\vec{b}}) = P^{\mathbf{G}\vec{b}}, \mathcal{E}(Z^{\vec{c}}) = Z^{(\mathbf{G}^{-1})^T \vec{c}}. \quad (3)$$

However, when \mathbf{G} is $M \times Q$ with $M > Q$, the parity information cannot be represented as a Z-string operator due to the lack of a left inverse. Instead, Z-string representation is discarded via $Z^{\vec{c}} P^{\vec{b}} = (-1)^{\vec{c} \cdot \vec{b}} P^{\vec{b}}$, leading to the following decomposition of \hat{O} :

$$\text{Re/Im}\{\hat{O}\} = X^{\vec{a}} \sum_{\vec{b} \in S_{\hat{O}}} (-1)^{\vec{c} \cdot \vec{b}} (P^{\vec{b}} \pm P^{(\vec{a} \oplus \vec{b})}), \quad (4)$$

$$\text{Re/Im}\{\mathcal{E}(\hat{O})\} = X^{\mathbf{G}\vec{a}} \sum_{\vec{b} \in S_{\hat{O}}} (-1)^{\vec{c} \cdot \vec{b}} (P^{\mathbf{G}\vec{b}} \pm P^{\mathbf{G}(\vec{a} \oplus \vec{b})}). \quad (5)$$

Fermionic encoding and decoding—The connection between operator encoding and linear code allows us to incorporate classical encoding-decoding methods to compute fermionic expectation values. Encoding now amounts to finding \mathbf{G} , which preserves $S_{\hat{O}}$, and the decoder $\mathbf{G}\vec{b} \rightarrow \vec{b}$. The parity check code of CEC turns out to be the right candidate for this task. It distinctively encodes fixed Hamming weight \vec{b} bit-flip errors and decodes them in polynomial time.

This property coincides with the particle-conserved constraint. Those bit-flip errors are dual to fermionic states, such that a code with distance $2N + 1$ CEC has a parity check matrix that distinctively encodes a number-conserved fermionic state. By applying the GV bound to the CEC code, we obtain an upper bound on the minimal size of the fermionic encoder, leading to our first result.

Theorem 1. *The minimal qubit cost required to encode an M fermionic modes N electrons problem has an upper bound of $Q \leq 2N \log M$.*

Proof. See Appendix C. □

This theorem guarantees the existence of a logarithmic mode scaling linear encoder. Scalable construction of such encoders can be outsourced. Existing LDPC code packages such as AFF3CT [28] and OpenFEC [29] can generate not only scalable GV bound-converging encoders but also polynomial-time decoders. To study the impact of the optimal encoder on quantum chemistry problems, we introduce the RLE algorithm in Appendix G. The compression rates of RLE Q/M are presented in Figure 3 and Table III.

Meanwhile, error decoding in CEC can be translated to fermionic state decoding for quantum simulation with a caveat. Unlike classical decoding, the expectation values of \hat{O} are decoded in multiple measurement bases, which contributes to the measurement complexity. To calculate the total measurement complexity, we note that $\text{Re/Im}\{\hat{O}\}$ in Eqn~(5) can be expanded as commuting Pauli strings measurable in one basis. It leads to the following measurement cost:

Theorem 2. *The number of Clifford bases for measuring the expectation value of a quantum chemistry Hamiltonian is upper bounded by $O(M^4)$.*

Proof. See Appendix D. \square

Both theorems assure the existence of an encoder with optimal qubit-to-measurement complexity trade-off. The final probability distributions requires decoding to avoid exponential Pauli expansion of $\mathcal{E}(\hat{O})$, a problem manifested in QEE. This is where we introduce FED [30] in Algorithm 1, which decodes the probability distributions of the projectors $X^{\mathbf{G}\vec{a}}(P^{\mathbf{G}\vec{b}} \pm P^{\mathbf{G}(\vec{a}\oplus\vec{b})}) \rightarrow X^{\vec{a}}(P^{\vec{b}} \pm P^{\vec{a}\oplus\vec{b}})$ with the aid of Clifford transformation \mathbf{A} in post-processing.

Algorithm1 Fermionic Expectation Decoder

Input: Probability distribution of projector variable $P(\vec{d} \in \mathbb{F}_2^Q)$, X -string vector \vec{a} of \hat{O} , Z -string vector \vec{c} of \hat{O} , Parity Check Matrix \mathbf{G} , Minimal Weight Decoder $F(\cdot)$

Output: Fermionic Expectation Value $\langle \hat{O} \rangle = \text{val}$

```

 $\vec{e} \leftarrow \vec{0} \in \mathbb{F}_2^Q;$ 
 $k \leftarrow \min \{k, \vec{a}[k] = 1\};$ 
 $\vec{e}[k] \leftarrow 1;$ 
Find  $\mathbf{A}$  s.t.  $\mathbf{A}\vec{e} = \mathbf{G}\vec{a};$ 
 $\text{val} = 0;$ 
for  $P(\vec{d}) \neq 0$  do
   $\vec{m} \leftarrow \mathbf{A}\vec{d};$ 
   $\vec{b} \leftarrow F(\vec{m});$ 
  Post-Select  $\vec{b}$  which obeys the number conservation constraint.
   $s \leftarrow (-1)^{\vec{b}\cdot\vec{c}} * (-1)^{\vec{d}[k]};$ 
   $\text{val} \leftarrow \text{val} + P(\vec{d}) * s;$ 
end for
return  $\text{val}$ 

```

Result—We benchmark the RLE-FED protocol on VQE and study its impact on gate resources and convergence w/o noise. In Figures 1 and 2, we conduct a case study of an 8-mode, 2-electron LiH molecule [31] in the STO-3G basis, compressed to 6 qubits at a bond length of 2.5 Å compressed to the JW encoded LiH using HEA, and examine a 12-mode, 2-electron H₂ molecule [32] in the 6-311G* basis, compressed to 7 qubits at bond lengths ranging from 0.5 to 2.5 Å. All data points represent averages over 30 instances of gradient descent; they are trained with HEA and Hartree-Fock initial state

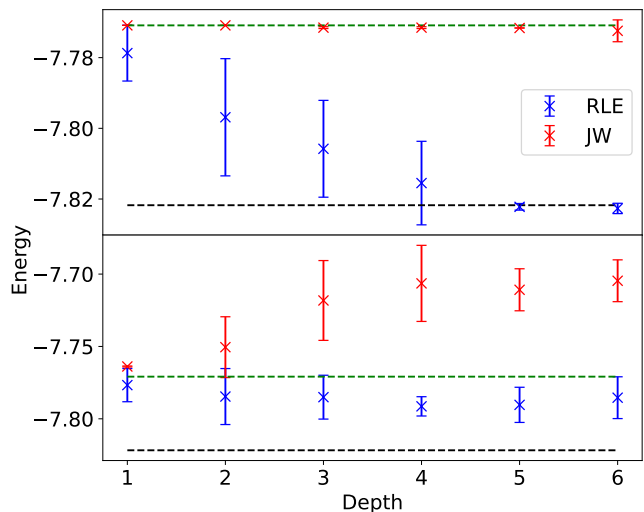


FIG. 1. This figure compares VQE energy of STO-3G LiH at 2.5 Å w/o compression using HEA at varying depth. The JW encoded noiseless energy (top red) cannot find energy better than the HF energy (green), whereas the RLE energy (blue) converges to chemical accuracy (black) at the 5th layer (25 CNOT). In the `ibm-sherbrooke` noisy simulation, the RLE energy shift is significantly less than the JW energy which diverges from the HF energy.

near zero parameters using the L-BFGS-B optimizer to account for the randomness of our encoder and the quantum noise.

For the RLE encoded problem, the LiH energy converges to chemical accuracy ($<1\text{kcal/mol}$) with 30 local CNOT gates. Similarly, the noisy simulation shows better convergence of the RLE encoded circuit due to reduced CNOT noise and better representation of the number-conserved subspace. The JW encoded LiH problem not only requires more entangling gates but also fails to show signs of convergence. Meanwhile, the H₂ energy converges using as few as 66 local CNOT gates, compared to the JW encoded H₂ which requires 11 CNOT gates at least per layer, and double excitations which requires at least 13 CNOT gates. Training the JW encoded LiH and H₂ molecules with HEA or the UCCSD ansatz requires significantly more CNOT gates to achieve the same accuracy. Subspace encoding allows state preparation with substantially less coherence time and consequently less circuit depth [33]. This is further supported with the benchmarks of 16-mode 6-31G LiH in Tables III and IV in Appendix F.

Overall, successful ansatz training on the RLE encoded circuit demonstrates significantly fewer CNOT gates, and consequently, the spatial and temporal aspects of the quantum circuits are less prone to noise than the uncompressed case. Noisy energy variance shows that the compressed problem also produces a stable result. Not only does our protocol help to minimize the effect of noise for preparing a VQE problem, it also allows for a more

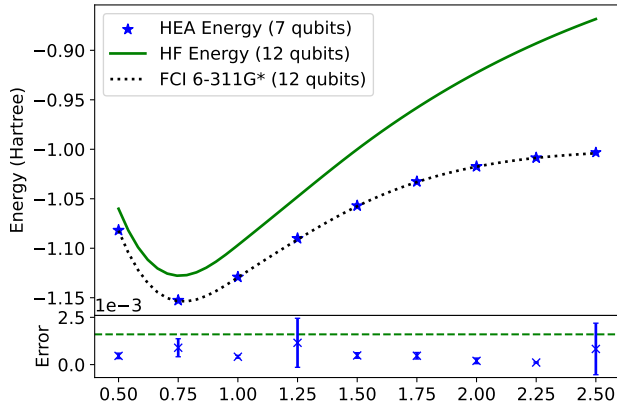


FIG. 2. This figure showcases the noiseless VQE potential energy curve of 6-311G* (12 modes) H_2 potential energy curves encoded with 7 qubits using HEA with 11 layers (66 CNOT). The energy uncertainty is displayed at the bottom corresponds which lies within the chemical accuracy threshold (green dot).

effective ground state preparation; and therefore is an effective tool that can comprehensively enhance the quality of the gradient descent.

Complexity Analysis – The RLE encoder and its associated classical decoder have a computational complexity of $\mathcal{O}(M^N)$. In practice, they are replaced with polynomial encoder-decoder constructions that attain the GV bound, such as the Goppa code and Gallager’s LDPC code. FED, when combined with optimal CEC, is fully scalable.

While our protocol has scalable encoding-decoding complexity, it does not directly address the encoded fermionic gate complexity. In fact, if we directly exponentiate the operator of Eqn~(5), the worst-case gate complexity scaling $\mathcal{O}(M^N)$, as shown in Appendix D. Unlike the segment code and Polylog scheme, RLE encoder has no gate related constraints. However, there are two ways to circumvent this problem.

Firstly, we can implement quantum algorithms without fermionic gates, such as our VQE benchmarks. Beyond NISQ algorithms, scalable gate implementation requires partial quantum state decoding $\mathcal{E}(|\psi\rangle) \rightarrow |\psi\rangle$ where only the necessary fermionic modes are decoded. Such a decoder will require $\mathcal{O}(\log M)$ (see Appendix E) ancillary

qubits and can be constructed with a variational quantum autoencoder (VAE) [34]. Similar to FED, which avoids exponential Pauli decomposition, a quantum decoder for encoded Fock bases can bypass the direct implementation of exponentially many commuting Pauli gates or multi-control gates. In practice, such a decoder is useful for designing sparse access oracles \hat{O}_H and \hat{O}_F [35] in compressed Fock bases to determine amplitudes $\langle \vec{a} | \hat{H} | \vec{b} \rangle$ and columns $\vec{f}(\vec{a}, l)$, where l is the l th non-zero element in the matrix row \vec{a} in the Fock basis.

Ultimately, it is possible to implement scalable fermionic gates in our scheme. However, it requires a quantum state decoder.

Conclusion – In this Letter, we have proposed parity check matrix and FED protocol for simulating particle-conserved fermionic problems. We established a connection between particle-conserved linear encoding and the parity check matrix of a dual CEC code, leading to an innovative protocol for constructing particle-conserved codes. Leveraging this duality, we demonstrated that the optimal number-conserved linear encoding is bounded above by $2N \log M$. Our proposed protocol prepares efficient measurement bases for fermionic observables, including the 2-RDM for quantum chemistry, with a measurement complexity upper bound of $1 + \binom{M}{2} + \binom{M}{4}$ using Clifford transformation. These bounds represent the optimal qubit-to-measurement trade-off for fermionic encoding and raise the question of whether this code can be efficiently solved.

The Geometric Goppa and Gallager’s LDPC codes are scalable examples which can attain the optimal compression scaling. To benchmark optimal codes, we constructed the RLE encoding and FED decoding algorithms. We conducted a VQE experiment on H_2 in the 6-311G* basis against FCI, demonstrating chemical accuracy across all bond lengths. We compared the VQE simulation on LiH in the RLE and JW encoded STO-3G/6-31G basis, and H_2 in the RLE encoded 6-311G* basis using HEA at different circuit depths. All results favored the optimal encoding in terms of CNOT cost and convergence, which showcased the potential benefits of implementing VQE with our protocol. Linear encoder could be extended for encoding quantum algorithms, provided that the sparse Hamiltonian can be approximated with quantum signal processing (QSP) strategies. We leave it an open question of how to accommodate optimal linear encoding with general quantum algorithms.

[1] B. Bauer, S. Bravyi, M. Motta, and G. K.-L. Chan, *Chem. Rev.* **120**, 12685 (2020).
 [2] A. Kitaev and C. Laumann, (2009), arXiv:0904.2771.
 [3] C. W. Bauer, Z. Davoudi, A. B. Balantekin, T. Bhattacharya, *et al.*, *PRX Quantum* **4**, 027001 (2023).
 [4] A. Ho, J. McClean, and S. P. Ong, *Joule* **2**, 810 (2018).
 [5] R. Santagati, A. Aspuru-Guzik, R. Babbush, M. Deg-

roote, *et al.*, (2023), arXiv:2301.04114.
 [6] J. Zhang, P. W. Hess, A. Kyprianidis, P. Becker, *et al.*, *Nature* **543**, 217 (2017).
 [7] R. P. Feynman, *Int. J. Theor. Phys* **21** (1988).
 [8] P. Jordan and E. P. Wigner, *Z. Phys.* **47**, 631 (1928).
 [9] M. Steudtner and S. Wehner, *New J. Phys.* **20**, 063010 (2018).

- [10] S. Bravyi, J. M. Gambetta, A. Mezzacapo, and K. Temme, (2017), [arXiv:1701.08213](https://arxiv.org/abs/1701.08213).
- [11] W. Kirby, B. Fuller, C. Hadfield, and A. Mezzacapo, *PRX Quantum* **3**, 020351 (2022).
- [12] Y. Shee, P. K. Tsai, C. L. Hong, H. C. Cheng, and H. S. Goan, *Phys. Rev. Res.* **4**, 023154 (2022).
- [13] W. J. Huggins, J. R. McClean, N. C. Rubin, Z. Jiang, *et al.*, *Npj Quantum Inf.* **7**, 23 (2021).
- [14] J. T. Seeley, M. J. Richard, and P. J. Love, *J. Chem. Phys.* **137**, 224109 (2012).
- [15] J. J. Shepherd, A. Grüneis, G. H. Booth, G. Kresse, and A. Alavi, *Phys. Rev. B* **86**, 035111 (2012).
- [16] A. Grüneis, J. J. Shepherd, A. Alavi, D. P. Tew, and G. H. Booth, *J. Chem. Phys.* **139**, 084112 (2013).
- [17] K. Bharti, A. Cervera-Lierta, T. H. Kyaw, T. Haug, *et al.*, *Rev. Mod. Phys.* **94** (2022).
- [18] T.-C. Yen, R. A. Lang, and A. F. Izmaylov, *J. Chem. Phys.* **151** (2019).
- [19] E. N. Gilbert, *Bell Labs Tech. J* **31**, 504 (1952).
- [20] R. R. Varshamov, *Dokl. Akad. Nauk SSSR* **117**, 739–741 (1957).
- [21] G. Katsman, M. Tsfasman, and S. Vladut, *IEEE Trans. Inf. Theory* **30**, 353 (1984).
- [22] S. Porter, B.-Z. Shen, and R. Pellikaan, *IEEE Trans. Inf. Theory* **38**, 1663 (1992).
- [23] R. Gallager, *IEEE Trans. Inf. Theory* **8**, 21 (1962).
- [24] J. Mosheiff, N. Resch, N. Ron-Zewi, S. Silas, and M. Wootters, *SIAM Journal on Computing* **0**, FOCS20 (2000).
- [25] G. H. Low and I. L. Chuang, *Phys. Rev. Lett.* **118**, 010501 (2017).
- [26] A. Kandala, A. Mezzacapo, K. Temme, M. Takita, M. Brink, J. M. Chow, and J. M. Gambetta, *Nature* **549**, 242 (2017).
- [27] X. Zeng, Y. Fan, J. Liu, Z. Li, and J. Yang, *J. Chem. Theory Comput.* **19**, 8587 (2023).
- [28] A. Cassagne, O. Hartmann, M. Léonardon, K. He, *et al.*, *SoftwareX* **10**, 100432 (2019).
- [29] J. R. McClean, K. J. Sung, I. D. Kivlichan, Y. Cao, *et al.*, *Quantum Sci. Technol.* **5**, 034014 (2020).
- [30] M. H. Cheng and A. C. Medina, <https://github.com/Tcsg22/RLE-FED-protocol-demo> (2024).
- [31] J. E. Rice, T. P. Gujarati, M. Motta, T. Y. Takeshita, *et al.*, *J. Chem. Phys.* **154**, 134115 (2021).
- [32] J. Du, N. Xu, X. Peng, P. Wang, *et al.*, *Phys. Rev. Lett.* **104**, 030502 (2010).
- [33] J. R. McClean, S. Boixo, V. N. Smelyanskiy, R. Babbush, and H. Neven, *Nat. Commun.* **9** (2018).
- [34] A. Rocchetto, E. Grant, S. Strelchuk, G. Carleo, and S. Severini, *Npj Quantum Inf.* **4**, 28 (2018).
- [35] D. Camps, L. Lin, R. Van Beeumen, and C. Yang, *SIAM J. Matrix Anal. Appl.* **45**, 801 (2024).
- [36] C.-K. Lee, C.-Y. Hsieh, S. Zhang, and L. Shi, *J. Chem. Theory Comput.* **18**, 2105 (2022), publisher: American Chemical Society.
- [37] F. J. MacWilliams and N. J. A. Sloane, *The Theory of Error Correcting Codes* (North-Holland Pub. Co., 1977).
- [38] S. B. Bravyi and A. Y. Kitaev, *Annals of Physics* **298**, 210 (2002).
- [39] R. Babbush, D. W. Berry, Y. R. Sanders, I. D. Kivlichan, *et al.*, *Quantum Sci. Technol.* **3**, 015006 (2017).
- [40] W. M. Kirby, S. Hadi, M. Kreshchuk, and P. J. Love, *Phys. Rev. A* **104**, 042607 (2021).
- [41] R. Babbush, D. W. Berry, Y. R. Sanders, I. D. Kivlichan, *et al.*, *Quantum Sci. Technol.* **3**, 015006 (2017).
- [42] I. O. Sokolov, P. K. Barkoutsos, P. J. Ollitrault, D. Greenberg, *et al.*, *J. Chem. Phys.* **152** (2020).
- [43] V. Pless, “Introduction to the theory of error-correcting codes,” (John Wiley /& Sons, Ltd, 1998) Chap. 1, pp. 1–15.
- [44] V. Pless, “Introduction to the theory of error-correcting codes,” (John Wiley /& Sons, Ltd, 1998) Chap. 2, pp. 17–38.
- [45] F. Hernando, F. D. Igual, and G. Quintana-Ortí, *ACM Trans. Math. Softw.* **45** (2019), 10.1145/3302389.

Appendix A: Framework for number-conserved Linear Encoding

We provide a detailed discussion of the dual code correspondence that connects number-conserved linear encoding with classical error-correcting codes, inspired by Ref. [10].

In this work, we make use of a $Q \times M$ parity check code \mathbf{G} of an $M - Q \times M$ CEC \mathbf{C} to compress the number-conserved configurations. \mathbf{G} is defined as the dual code of \mathbf{C} :

$$\mathbf{G}\mathbf{C}^T = \mathbf{0}. \quad (\text{A1})$$

Due to this duality, constraints on \mathbf{P} can be directly translated to constraints in \mathbf{C} . With respect to \mathbf{G} , we can think of \mathbf{C} as the generator of equivalence class C on the M -dimensional binary vector space \mathbb{F}_2^M :

$$C = \{\vec{v} \in \mathbb{F}_2^M \mid \forall \vec{c} \in \mathbb{F}_2^{M-Q}, \vec{v} = \mathbf{C}^T \vec{c}\} = \ker \mathbf{G}. \quad (\text{A2})$$

This class C is the kernel $\ker \mathbf{G}$ of the encoded space. $\ker \mathbf{G}$ also defines the equivalence class of all encoded bitstrings $\vec{b} \in \mathbb{F}_2^M$:

$$\vec{b} \sim \vec{b} \oplus \vec{v} \text{ for } \vec{v} \in C. \quad (\text{A3})$$

Let us define $\vec{b} \oplus C$ to be the equivalence class of \vec{b} . To ensure that all configurations are distinctly encoded, number-conservation demands that each bitstring with Hamming weight N shall only appear once in $\vec{b} \oplus C$, which constrains the Hamming weight of C and thus its generator \mathbf{C} , the error-correcting code. If \mathbf{C} generates a subspace of even Hamming weights with code distance $2N+2$, then for the subspace with Hamming weight less than or equal to N , \mathbf{G} will distinctively encode them into the encoded space. Proof of this statement is in Lemma 1. On the other hand, we can generate arbitrary odd equivalence classes because they do not contribute to mapping bitstrings with the same parity.

As we will show in the proof of Theorem 1, this is equivalent to saying that we would like our \mathbf{C} to have one unconstrained row element with odd Hamming weight. As for the rest of the rows, they form a code with even Hamming weight and distance $2N+2$. Thus, \mathbf{C} contains an error-correcting subcode of dimension $(M - Q - 1) \times M$ with even Hamming weight and distance $2N+2$ for us to construct a valid $Q \times M$ number-conserved linear encoding with code parameters $[M, M - Q - 1, 2N + 2]$.

Appendix B: Framework for Qubit Operator Encoding

The basics of operator encoding-decoding is reviewed here in the language of binary linear vector space. Literature such as Ref. [12] and [36] employ projectors for approaching the $\lceil N \log M \rceil$ lower bound. However, both methods suffer from unscalable measurement costs. One reason behind this broken scaling is the disruption of the linear structures of the projectors. In our framework, we connect the projector to linear binary vector space, which allows us to assess the measurement complexity with the linear structure.

1. Notations and Properties

We define the notations of the X , P , Z -strings used in this paper.

Definition 1. *Projectors in the computational basis are defined as:*

$$P^{0/1} = |0/1\rangle\langle 0/1| = \frac{1 + (-1)^{0/1}Z}{2} \quad (\text{B1})$$

Definition 2. *Let $\vec{b} \in \mathbb{F}_2^M$ be a binary vector, P -string is defined as follows:*

$$P^{\vec{a}} = \prod_{m=1}^M P_m^{\vec{b}[m]}. \quad (\text{B2})$$

with $\vec{b}[m]$ denotes the m th entry of the vector and the following property:

$$P^{\vec{b}} |\vec{a}\rangle = \delta_{ab} |\vec{a}\rangle. \quad (\text{B3})$$

Definition 3. *Let $\vec{b} \in \mathbb{F}_2^M$ be a binary vector, X -string is defined as follows:*

$$X^{\vec{b}} = \prod_{m=1}^M X_m^{\vec{b}[m]}. \quad (\text{B4})$$

with $\vec{b}[m]$ denotes the m th entry of the vector and the following property:

$$X^{\vec{b}} |a\rangle = |\vec{a} \oplus \vec{b}\rangle. \quad (\text{B5})$$

Definition 4. *Let $\vec{b} \in \mathbb{F}_2^M$ be a binary vector, we define a Z -string as follows:*

$$Z^{\vec{b}} = \prod_{m=1}^M Z_m^{\vec{b}[m]}. \quad (\text{B6})$$

with $\vec{b}[m]$ denotes the m th entry of the vector and the following property:

$$Z^{\vec{b}} |\vec{a}\rangle = (-1)^{\vec{b} \cdot \vec{a}} |\vec{a}\rangle. \quad (\text{B7})$$

Next, we will derive the transformation of the X , P , and Z -strings with an encoder $\mathcal{E} : |\vec{a}\rangle \rightarrow |\mathbf{G}\vec{a}\rangle$. Immediately, we can infer from the state encoding of operators in Eqns (B3), (B5), and (B7) the transformations as:

$$\mathcal{E}(P^{\vec{b}}) = P^{\mathbf{G}\vec{b}} \quad (\text{B8})$$

$$\mathcal{E}(X^{\vec{b}}) = X^{\mathbf{G}\vec{b}} \quad (\text{B9})$$

$$\mathcal{E}(Z^{\vec{b}}) = Z^{(\mathbf{G}^{-1})^T \vec{b}}. \quad (\text{B10})$$

Linear compression preserves Eqns (B8) and (B9), but breaks Eqn (B10) due to the lack of a left inverse for \mathbf{G} . Instead, the individual Pauli- Z operator can be encoded as:

$$\mathcal{E}(Z^{\vec{c}}) = \sum_{\vec{b} \in S} (-1)^{\vec{c} \cdot \vec{b}} P^{\mathbf{G}\vec{b}} \quad (\text{B11})$$

where $P^{\mathbf{G}\vec{b}}$ is a Q -qubit projector, and $S = \{\vec{b} \mid H(\vec{b}) = N\}$ is the set of all number-conserving states. The exact gate implementation of Eqn (B11) can be performed with multi-control gates or a linear combination of an exponential number of Z -strings. However, both methods suffer from scalability problems, as discussed in the gate complexity section in Appendix E. This problem can be tackled using QSP techniques, provided that the encoded $\mathcal{E}(Z^{\vec{c}})$ is also sparse.

2. XP Decomposition

We can now derive a general representation of the qubit operator. In essence, all qubit operators consist of a selected set of states, state transitions, and phase evolution. In the computational basis, X -strings capture transitions, Z -strings capture phase, and the sum over projectors captures the states.

Given an X -string $X^{\vec{a}}$ and a projector $P^{\vec{b}}$, we can observe the following properties:

$$X^{\vec{a}} P^{\vec{b}} = P^{\vec{a} \oplus \vec{b}} X^{\vec{a}} \quad (\text{B12})$$

We can represent the Hermitian or anti-Hermitian part of the operator as:

$$X^{\vec{a}} (P^{\vec{b}} \pm P^{\vec{a} \oplus \vec{b}}) = |\vec{a} \oplus \vec{b}\rangle \langle \vec{b} | \pm | \vec{b} \rangle \langle \vec{a} \oplus \vec{b} | \quad (\text{B13})$$

$$(X^{\vec{a}} (P^{\vec{b}} \pm P^{\vec{a} \oplus \vec{b}}))^{\dagger} = \pm X^{\vec{a}} (P^{\vec{b}} \pm P^{\vec{a} \oplus \vec{b}}). \quad (\text{B14})$$

Summation over this basis operator with respect to the Boolean vector \vec{a} and \vec{b} allows us to construct arbitrary (anti-)Hermitian qubit operators. As we show in Theorem 2, arbitrary sum over projector $P^{\vec{b}}$ and its conjugate $P^{\vec{a} \oplus \vec{b}}$ and $X^{\vec{a}}$ generates commuting Pauli strings as we expand the projector into Z -strings. The number of X -strings determines the measurement cost of a given qubit operator. Suppose now we exponentiate the Hermitian

operator. It also determines the Trotterization steps required to approximate the unitary evolution.

In the JW representation, the product of creation and annihilation operators always generates one X -string under our decomposition. Our linear encoder then surjectively encodes the JW X -strings. This property allows us to exactly implement fermionic gates, though at the risk of an unscalable number of gates, and efficiently prepare measurement bases for fermionic observables.

Appendix C: Qubit Complexity Proof

Lemma 1. *Given bitwise linear map \mathcal{E} which is number-conserved, for all bitstrings k which is an element of $\ker \mathcal{E}$, $D_H(k, 0) \geq 2N + 2$ if $D_H(k, 0) \equiv 0 \pmod{2}$.*

Proof. This theorem claims that the even Hamming weight codewords, generated from the kernel space, must be lower bounded by $2N + 2$.

Suppose there is a bitstring \vec{k} with Hamming weight $2K < 2N + 2$. We can construct two distinct bitstrings with Hamming weight N such that $\vec{d} = \vec{c} \oplus \vec{k}$, and \vec{c}, \vec{d} have $N - K$ overlapping bits. We observe the following relation in the encoded space

$$\mathcal{E}(\vec{d}) = \mathcal{E}(\vec{c}) \oplus \mathcal{E}(\vec{k}) = \mathcal{E}(\vec{c}). \quad (\text{C1})$$

□

Theorem 1. *The minimal qubit cost required to encode a M fermionic modes N electrons problem has the upper bound of $Q \leq 2N \log M$.*

Proof. From Theorem 1, we observe that all even kernel elements k , generated by the dual code \mathbf{C}^T , have even Hamming weight lower bounded as $D_H(k, 0) \geq 2N + 2$. We can interpret the row of \mathbf{C} as a $M - Q$ set of M -bit bitstrings, whose arbitrary bitwise addition \oplus among the bitstrings are encoded into the $\mathbf{0}$ vector in the encoded space. Since \mathbf{C} is invariant under elementary bitwise row addition, it is possible to eliminate the odd Hamming weight M -bit bitstrings with odd Hamming weight M -bit bitstrings. \mathbf{C} can be reorganized as a set of M -bit bitstrings with *only one* element with odd Hamming weight. In this form, we can impose Theorem 1 on the $M - Q - 1$ numbers of M -bit bitstrings.

Next, we reformulate the constraint as finding the maximal $M - Q - 1$ of \mathbf{C} given qubits M , and minimal hamming distance $2N + 2$, and all Hamming weight of elements in \mathbf{C} are even. Borrowing from CEC, the maximum is upper bounded by the Hamming bound [37] and lower bounded

by the Gilbert–Varshamov bound [19, 20].

$$\frac{2^{M-1}}{\sum_{j=0}^N \binom{M}{2j}} \leq 2^{M-Q-1} < \frac{2^{M-1}}{\sum_{j=0}^{\lfloor \frac{N}{2} \rfloor} \binom{M}{2j}} \quad (\text{C2})$$

$$\begin{aligned} M - 1 - \log \sum_{j=0}^N \binom{M}{2j} &\leq M - Q - 1 \\ &< M - 1 - \log \sum_{j=0}^{\lfloor N/2 \rfloor} \binom{M}{2j} \\ 2N \log M &\geq Q > 2 \left\lfloor \frac{N}{2} \right\rfloor \log M. \end{aligned} \quad (\text{C3})$$

We modify the Hamming and Gilbert–Varshamov bound in Eqn~(C2) such that we are only considering the bound on the even Hamming weight subspace, which has size 2^{M-1} ; and the sum $\sum_{j=0}^N \binom{M}{2j}$ is only over the even binomial coefficients. However, the argument of the Hamming cube as the maximal non-overlapping covering remained unchanged [19]. We also note that the Hamming bound for even subspace becomes a strict non-equality because the covering space does not cover the whole even code subspace.

We have proved that optimal bitwise linear encoding has $\mathcal{O}(N \log M)$ scaling. In particular, the lower bound coincides with the scaling of physical states. □

Appendix D: Proof for Measurement Complexity

Lemma 2. *All fermionic operators that can be written as a product of creation and annihilation operators can be expressed in terms of the product of one X -string and sum over P -strings under linear compression.*

Proof. Let us consider the Jordan–Wigner basis. The one particle creation and annihilation operators are written as the product of the Pauli-Z operator Z_m , Pauli-X operator X_i , and projector $P_i^{0/1}$ defined in Definition B1:

$$\hat{a}_i^\dagger = \prod_{m=1}^{i-1} Z_m X_i P_i^0 \quad (\text{D1})$$

$$\hat{a}_j = \prod_{m=1}^{j-1} Z_m X_j P_j^1. \quad (\text{D2})$$

Using the completeness relation of the identity operator, it is possible to expand $P_i^{0/1}$ as a sum over projector strings $P^{a_1 a_2 \dots a_{M-1}}$ defined in Def. 2:

$$P_i^{0/1} = P_i^{0/1} \otimes \sum_{\vec{a} \in \{0,1\}^{M-1}} P^{\vec{a}}. \quad (\text{D3})$$

Thus, the Z -strings, $\prod_{m=1}^{i-1} Z_m$ from the above example, can be absorbed into the projectors via the relationship:

$$Z^{\vec{c}} P^{\vec{b}} = (-1)^{\vec{c} \cdot \vec{b}} P^{\vec{b}}. \quad (\text{D4})$$

After this procedure, fermionic observables can be represented with only the X-strings, projectors, and signs. Each projector represents a fermionic state, and the unphysical states are discarded such that the encoded projectors would not coincide with the number-conserved projectors due to the equivalent classes. Let us denote \hat{O} as the product of creation and annihilation operators. Given a linear encoder $\mathcal{E}(\cdot)$ we can succinctly express the unencoded and encoded gates as follows:

$$\hat{O} = X^{\vec{a}} \sum_{\vec{b} \in S_{\hat{O}}} (-1)^{\vec{c} \cdot \vec{b}} P^{\vec{b}} \quad (\text{D5})$$

$$\mathcal{E}(\hat{O}) = X^{\mathbf{G}\vec{a}} \sum_{\vec{b} \in S_{\hat{O}}} (-1)^{\vec{c} \cdot \vec{b}} P^{\mathbf{G}\vec{b}} \quad (\text{D6})$$

where $S_{\hat{O}}$ represents the set of number-conserved states on which \hat{O} acts, and $\vec{a}, \vec{c} \in \mathbb{F}_2^M$ are binary vector uniquely associated with each operator \hat{O} , and \vec{a} induces physical state transition and \vec{c} encodes the sign information for each vector \vec{b} . \square

Lemma 3. *The real and imaginary part of an observable $\text{Re/Im}\{\hat{O}\}$ of the form in Eqn~(D6) can be measured with one measurement basis under linear encoding.*

Proof. From Eqn~(B14) and Eqn~(D6), we can write the (anti-)Hermitian part of the operators as Eqn~(5):

$$\text{Re/Im}\{\mathcal{E}(\hat{O})\} = X^{\mathbf{G}\vec{a}} \sum_{\vec{b} \in S_{\hat{O}}} (-1)^{\vec{c} \cdot \vec{b}} (P^{\mathbf{G}\vec{b}} \pm P^{\mathbf{G}(\vec{a} \oplus \vec{b})}). \quad (\text{D7})$$

We make use of the following CNOT transformation to eliminate the extra Pauli-X operations:

$$\text{CNOT}_{1,2} X_1 X_2 \text{CNOT}_{1,2} = X_1 \quad (\text{D8})$$

$$\text{CNOT}_{1,2} P^{a_1 a_2} \text{CNOT}_{1,2} = P^{a_1 (a_1 \oplus a_2)} \quad (\text{D9})$$

where we define i as control qubit and j as target qubit for $\text{CNOT}_{i,j}$. Applying the Eqn~(D9) on a pair of conjugate projectors in the form of Eqn~(B14), we observe that the projector at the target qubit will have the same parity. The full set of CNOT gates \hat{C} results in the following transformation:

$$\hat{C} X^{\mathbf{G}\vec{a}} \hat{C}^\dagger = X_B \quad (\text{D10})$$

$$\hat{C} P^{\mathbf{G}\vec{b}} \hat{C}^\dagger = P^{\mathbf{M}\mathbf{G}\vec{b}} = P_B^0 P^{\vec{m}} \quad (\text{D11})$$

$$\hat{C} P^{\mathbf{G}(\vec{a} \oplus \vec{b})} \hat{C}^\dagger = P^{\mathbf{M}\mathbf{G}(\vec{a} \oplus \vec{b})} = P_B^1 P^{\vec{m}} \quad (\text{D12})$$

where the adjoint action of \hat{C} on P is equal to the $Q \times Q$ matrix \mathbf{M} action on $\mathbf{G}\vec{b}$, such that $\mathbf{M}\mathbf{G}(n\vec{a}) \oplus \vec{b} = ((n \bmod 2)_B, \vec{m}(\vec{b}))$, with B denoting the bit location on which X_B acts and n an integer. We write $\vec{m} = \vec{m}(\vec{b})$ as a function of \vec{b} to simplify the notation in the sum. The operator becomes:

$$\hat{C} \text{Re/Im}\{\mathcal{E}(\hat{O})\} \hat{C}^\dagger = \sum_{\vec{b} \in S_{\hat{O}}} (-1)^{\vec{c} \cdot \vec{b}} X_B (P_B^0 P^{\vec{m}(\vec{b})} \pm P_B^1 P^{\vec{m}(\vec{b})}) \quad (\text{D13})$$

On qubit B , the sum of P^0 and P^1 generates local I or difference generates Z_N . We can rewrite them as X_N or $-iY_N$, as shown in Eqn~(E1).

Since all operators, except the qubit Q which is either X_i when hermitian or iY_Q otherwise, are projectors made of I, Z operators, the real/imaginary part of the bitwise linear encoded operators must generate commuting Pauli string in the Clifford transformed basis. Finally, since Clifford transforms one-to-one encoded Pauli strings, the operator $\text{Re/Im}\{\mathcal{E}(\hat{O})\}$ also generates commuting Pauli strings. \square

Theorem 2. *The number of Clifford bases for measuring the expectation value of a quantum chemistry Hamiltonian is upper bounded by $\mathcal{O}(M^4)$.*

Proof. We only need to determine the measurement complexity of 2-RDM.

Next, from Lemma 2 and 3, we see that the (anti-)Hermitian part of the 2-RDM, defined as $\langle \psi | \hat{a}_i^\dagger \hat{a}_j^\dagger \hat{a}_k \hat{a}_l \pm \hat{a}_l^\dagger \hat{a}_k^\dagger \hat{a}_j \hat{a}_i | \psi \rangle$, can be measured in one basis for each set of fermionic modes i, j, k, l . In quantum chemistry, we are only interested in the real part of the observables. Therefore, each i, j, k, l demands one measurement basis.

Due to the result in Lemma 3, each distinct X-string corresponds to one unique measurement basis. Upon encoding the 2-RDM operator via the JW transformation, we see that the encoded operator is of the form of the real part of Eqn~(D5). The X-string in this JW representation is invariant under any permutation among i, j, k, l in the JW representation. Thus, the measurement scaling is equal to the possible combinations of i, j, k, l , where we allow the indices to be equal to each other. Next, we count the number of distinct X-strings derived from the possible permutation. In the JW representation, when all indices are not equal to each other, the number of distinct X-strings corresponds to a complete set of M dimensional binary vectors with Hamming weight 4. Meanwhile, when one pair of indices share the same digit, it corresponds to the set of M dimensional binary vectors with Hamming weight 2. When two pairs are equal, then it corresponds to M dimensional binary vectors with Hamming weight 0. Under our formalism, each X-string can be associated with a binary vector. Thus, the total measurement cost, without parallelization [13], is equal to $\binom{M}{0} + \binom{M}{2} + \binom{M}{4}$. Parallelization is the simultaneous measurement of two or more sets of RDM elements with non-overlapping indices, maximal linear encoding breaks parallelization.

Finally, since a linear compression surjectively encodes the X-string guaranteed by the $2N + 2$ code distance of the CEC \mathbf{C} , $\binom{M}{0} + \binom{M}{2} + \binom{M}{4}$ is the upper bound of the measurement scaling for the encoded space. \square

Corollary 1. *The scaling of measurement basis can be completely characterized by the number of distinct X-strings that appears in the X and P decomposition.*

Proof. From the previous proof, each unique X-string, obtained from the X P decomposition of an operator, generates commuting Pauli strings. Meanwhile, Pauli strings generated by two distinct X-strings, and two pairs of respective projectors, contain mutually non-commuting terms. \square

This result can also be employed to characterize non-linear encoding, which *does not* surjectively encode X strings to X strings. Instead, Eqn~(D7) will further split into a sum over X strings. Scalable measurement is still possible if the distinct X strings for each single/double excitation operators scales polynomially.

Appendix E: Fermionic Gate Complexity

Under the same framework, we show that linear encoding allow exact implementation of real or imaginary parts of the single and double excitation \hat{O} in Eqn~(D6). This is a feature that is impossible for any non-linear encoding, where \hat{O} is represented with more than one type of X-string under our XP decomposition. As a result, trotterisation is required to approximate \hat{O} compared to linear encoding. However, this property does not save linear encoders from unscalable gate complexity in exact gate implementation.

Proposition 1. *The fermionic gate of single and double excitations can be decomposed as a series of multi-control gates and Clifford gates.*

Proof. From Lemma 3, we can transform operators in Eqn~(D7) into X-string with the Clifford transformation \hat{C} and operator of the form:

$$\hat{C} \text{Re/Im}\{\mathcal{E}(\hat{O})\}\hat{C}^\dagger = \sum_{\vec{m} \in S_{\hat{O}}} X_B / -iY_B P^{\vec{m}(\vec{b})} \quad (\text{E1})$$

where $X_B / -iY_B$ is the last Pauli-X/Y operator at qubit B. For the implementation of fermionic gates, it is necessary to describe the exponentiation of this operator representation. \hat{C} , described in Eqns~(D10), (D11), and (D12), survives under exponentiation. Meanwhile, each operator $X_N / -iY_N P^{\vec{m}(\vec{b})}$ is mutually commutative, and its exponentiation corresponds to a multi-control X/Y rotation, with the projectors acting as the control bits. Consequently, the exponentiation of the diagonalized fermionic operators can be represented as a product of multi-control Pauli-X/Y gates. \square

For molecular simulation, where only the real part of fermionic operators matters, the multi-control gates with a Clifford transformation can exactly implement fermionic gates defined in Lemma 2. However, the number of multi-control gates given by the size of $S_{\hat{O}}$ indicates that the worst-case scenario gate complexity has combinatorial scaling $\mathcal{O}(M^N)$ [10]. The number of multi-control gates can hypothetically be reduced by gate approximations or employing the completeness relation of

multi-control gates, where different controls can merge and cancel out each other based on their control state. However, classical parity check codes have no fermionic gate-related constraints on the encoder, making it difficult to expect any advantages in the scalable implementation of multi-control gates.

The segment code in Ref. [9] and Polylog code in Ref. [11] circumvent this problem by imposing constraints on the encoder. In particular, the segment code uses its block structure on the encoder to ensure that the N-particle states are mapped into N-particle states belonging to the set $S_{\hat{O}}$ in our notation. Although the corresponding explicit gate complexity is not specified, it is polynomial in both N and M based on the construction. Meanwhile, the Polylog code further exploits the block structure on the encoder and QSP to approximately implement the Z-strings. The single Pauli-Z operator is first encoded into a sum of Pauli-Z operators, rescaled by a cosine function necessary for the final QSP polynomial transformation, which maps the cosine eigenvalues to a step function, the desired property of an encoded Pauli-Z operator, with a gate complexity lower bounded by $\mathcal{O}(N^2 \log M^4)$.

These approaches offer solutions to the gate scalability problem. In general, the constraints on the encoder for scalable fermionic gate representation can be translated to whether the fermionic information, sign, and state, can be efficiently decoded from the encoded entangled state quantum mechanically. That is, the quantum analogy of our FED algorithm. Efficient constructions are available in existing techniques such as the variational quantum autoencoder (VAE) [34].

While typical quantum state decoding aims to decode the entire quantum state, in our context, only the fermionic sub-modes on which the local operator in the unencoded space acts require decoding for implementing fermionic gates. Therefore, this approach does not increase the scaling of our current qubit complexity. For example, the quantum version of post-selection of number-conserved states $|\vec{b}\rangle$ in Algorithm 1 requires decoding only the modes on which the double excitation creation operator acts, as well as two modes for the single excitation. Control operations can then be implemented on the decoded ancillary qubit to manage transitions on entangled states. In our FED algorithm, another necessary component for decoding is the sign information due to fermionic exchange symmetry. In the JW-encoded basis, specifying the sign information would require decoding up to $\mathcal{O}(M)$ modes, which is the resource requirement in our classical FED algorithm. However, in the BK-encoded basis, we only need to decode $\mathcal{O}(\log M)$ modes, as pointed out by Ref. [11]. Consequently, a quantum fermionic sign decoder would only require an additional $\mathcal{O}(\log M)$ BK modes [38], stored as the Z-string defined in Eqn~(3). Thus, the design of a fermionic mode decoder would require a total qubit complexity of $(2N + 1) \log M$, on top of the GV-bounded compression rate for linear codes.

Under our scheme, a quantum fermionic mode decoder is necessary for encoding quantum algorithms and for implementing fermionic gates. A key application is the block-encoding of the sparse access oracles \hat{O}_H and \hat{O}_F as discussed in Ref. [35]. In Ref. [39, 40], the implementation of second-quantized QSP in the number-conserved subspace requires a redefinition of the Fock basis for the scalable \hat{O}_H and \hat{O}_F . A quantum decoder can avoid such a construction and provide more flexible means of encoding the fermionic problem. Moreover, when the quantum decoder is incorporated into QSP, quantum simulation on arbitrary fermionic sparse matrices becomes possible. Following the argument in Ref. [41] and the GV bound, the sparsity for fermionic simulation under this scheme is bounded by $d \leq 1 + \binom{2N}{1} \binom{M-2N}{1} + \binom{2N}{2} \binom{M-2N}{2} \in \mathcal{O}(N^2 M^2)$, leading to the polynomial query complexity of $\mathcal{O}(t N^2 M^2 \|\hat{H}\|_{\max} + \log(1/\epsilon)/\log \log(1/\epsilon))$.

Overall, given that classical LDPC decoders are naturally efficient, it is natural to expect a corresponding quantum fermionic sign decoder. For example, it is possible to train VAE decoders. While VAEs promise scalable gate implementation, their construction and corresponding complexity are beyond the scope of this work and are subject to future investigation. Overall, quantizing the classical parity check decoder is necessary for scalable gate implementation and fermionic quantum algorithm encoding.

Appendix F: Numerical Details

1. The Compression Rate

Numerical study of the compression rate Q/M given Q . This table directly compares to the Graph-Based encoding table in [10], which shows qubit advantages in all settings. Meanwhile, the polylogarithmic encoding cannot be compared with because their encoding advantage only appears in the 10^5 qubits regime. Logarithmic scaling in M means that it is possible to compress a large number of fermionic modes with a qubit cost that is manageable in the fault-tolerant regime. For instance, a 2-electron problem with 100 modes can be encoded with fewer than 20 qubits and a 4-electron problem with 400 modes in 50 qubits.

To analyze the scaling with respect to the number of modes, we evaluated the compression rate Q/M and presented the results in Figure 3 for a 4-electron problem. We benchmarked our results against the JW basis, graph-based encoding, and the theoretical upper and lower bounds. Our compression rate for linear encoding surpasses that of all previous works [10] across all scenarios. Compared to the non-linear QEE scheme, we maintain $\mathcal{O}(N \log M)$ scaling while achieving polynomial measurement scaling.

N \ M	Q										
	10	12	14	16	18	20	22	24	26	28	30
2	22	36	48	64	90	118	158	226	316	420	580
3	13	20	25	31	38	46	58	72	88	105	140
4	11	14	18	23	27	31	36	42	50	60	71
5	11	14	16	19	22	26	31	34	39	44	49
6	11	13	16	18	21	23	27	31	34	37	41

TABLE II. The numerical result of RLE compression. This table shows the maximum number of modes M that we can encode given the number of electron N (rows) and qubits Q (columns) with RLE. All results were computed on an 8-core laptop.

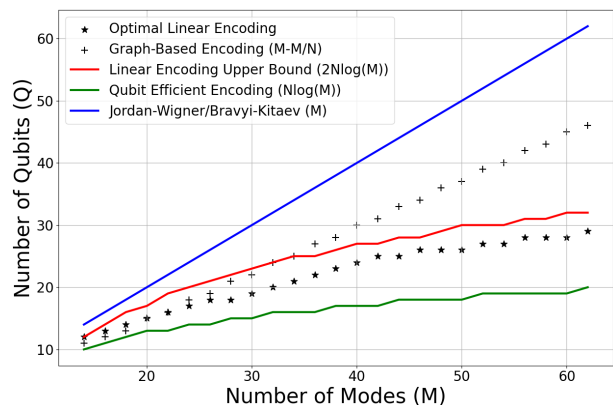
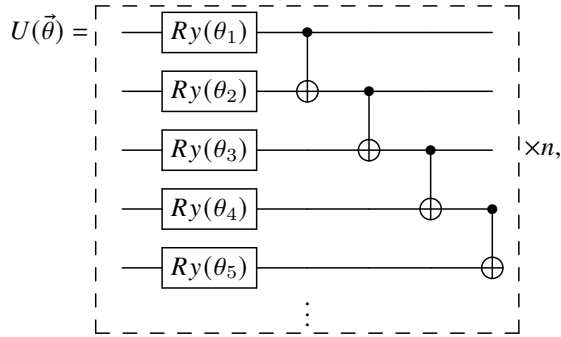


FIG. 3. Comparison of the qubit cost of RLE (star) to the JW basis (blue), graph-based encoding (cross), and QEE (green) for a 4 electron problem and the $2N \log M$ bound (red) against the number of orbitals.

2. Hardware-Efficient Ansatz

The Hardware-Efficient Ansatz (HEA) is commonly used in Variational Quantum Eigensolver (VQE) due to its resource efficiency given the current noisy constraints of quantum devices. Different hardware setups have their own specific HEA configurations, which include the selection of gates, circuit connectivity, and noise models. To meet these criteria, we design our HEA with two constraints. First, the gates used in our VQE simulations are restricted to the two-qubit Controlled-NOT gate and the single-qubit Y gate for rotations. Second, the connectivity of the two-qubit gates is constrained to a 1D chain topology. The design of the ansatz is therefore as follows:



the n is the number of repetitions of the circuit block.

3. Comparison with Unitary Couple Cluster type of Ansatz

We compared the performance of the Hardware-Efficient Ansatz (HEA) in the compressed space to the UCC-type Ansatz [42], which is the gold standard for computational chemistry simulations, specifically for the ground state simulation of LiH in the STO-3G and 6-31G basis sets. For the active space chosen as $M = 8$ and $M = 16$ fermionic modes respectively, we restricted the Hilbert space generated from both bases to the subspace of two electrons, denoted as (8,2) and (16,2).

In the STO-3G case, both the 6-qubit compressed and 8-qubit uncompressed Hamiltonians achieved chemical accuracy of 1 Kcal/mol using HEA with a reasonable circuit depth. However, the 6-qubit Hamiltonian achieved accuracy four orders of magnitude higher compared to the 8-qubit Hamiltonian, with fewer parameters and shallower circuit depth.

In contrast, the UCC-type ansatz converges faster and more easily compared to HEA, owing to its smaller number of parameters. However, achieving approximately one order of magnitude higher accuracy than HEA requires a circuit depth approximately two orders of magnitude deeper and roughly ten times more two-qubit gates.

Systems	LiH (8,2)			
	HEA		UCC	
Ansatz Types	8 qubits	6 qubits	SUCCD	UCCSD
Number of Parameters	48	36	6	15
Number of CNOT	35	25	480	768
Circuit Depth	41	31	668	1043
ΔE (kcal/mol)	0.4126	0.0002	0.5216	0.00003

TABLE III. This table showcases the noiseless simulation of (8,2) LiH using HEA and UCC-type ansatz on the state vector simulator. ΔE is the difference between the VQE energy and energy from exact diagonalisation. The HEA results are chosen from the lowest energy results using the VQE with L-BFGS-B optimizer and 100 different initial states. The UCCSD and SUCCD ansatz is constructed from Qiskit package

However, when scaling up to the (16,2) LiH system, the Hardware-Efficient Ansatz (HEA) applied directly to the uncompressed Hilbert space starts exhibiting Barren Plateaus. Even with L-BFGS-B optimization using 100 initial states, convergence to the required chemical accuracy is not achieved.

In contrast, using the RLE approach, which encodes the original 16-qubit Hamiltonian into an 8-qubit Hamiltonian, HEA can successfully converge to chemical accuracy.

Systems	LiH (16,2)			
	HEA		UCC	
Ansatz Types	16 qubits	8 qubits	SUCCD	UCCSD
Number of Parameters	96	48	28	63
Number of CNOT	75	35	4032	7280
Circuit Depth	81	41	4874	8675
ΔE (kcal/mol)	2.2099	0.7186	0.5749	0.00001

TABLE IV. This table showcases the noiseless simulation of (16,2) LiH using HEA and UCC-type ansatz on the state vector simulator. ΔE is the difference between the VQE energy and energy from exact diagonalisation. The HEA results are chosen from the lowest energy results using the VQE with L-BFGS-B optimizer and 100 different initial states. The UCCSD and SUCCD ansatz are constructed from the Qiskit package.

In conclusion, the LiH system scaling result shows that the qubit compression can improve VQE convergence while reducing the qubit cost and circuit depth.

Appendix G: Randomized Linear Encoder

1. The algorithm

RLE begins its random search by choosing a Q within the bounded region $N \log_2 M < Q < 2N \log_2 M$. Then, the algorithm initializes the parity check matrix $\mathbf{G} = [I_Q | D]$ in the *standard basis* [43, 44], where I_Q is a $Q \times Q$ identity matrix. The standard basis helps reduce the space of randomized search. We randomly generate the $Q \times (M - Q)$ matrix D such that each column has even Hamming weight equal to the value $Q/2$, denoted as $\text{even}(Q/2)$.

The second part of the algorithm consists of checks. Initially, the algorithm censors a large set of flawed generators by randomly verifying the Hamming weight of the element k generated by the $M - Q$ dimensional vector \vec{v} and the CEC \mathbf{C} .

$$\vec{k} = \mathbf{C}\vec{v}, \vec{v} \in S \quad (\text{G1})$$

where S is defined as the set of all vectors with Hamming weight 2 and $2K$ for $2K < N$, where K is a randomly generated integer. The random check serves to maximize the probability of obtaining the correct encoder. Finally, the algorithm explicitly computes the states to check for

Algorithm2 Randomized Linear Encoder

Input: Target States \mathbf{S} ; Testing subset T_s ;
Output: Codeword \mathbf{C} ;

```

while True do
  Initialized Codeword  $\mathbf{W} = []$ ;
  Random generate D with constraints;
   $\mathbf{G} \leftarrow [I_Q|D]$ ;
  Create distance  $2N + 2$  error correction matrix  $C \leftarrow [-D^T|I_{M-Q}]$ ;
  Create a checking list  $w = []$ 
  for  $t_s$  in  $T_s$  do
     $w \leftarrow [w|D_H(\sum C^T(t_s) \bmod 2, \mathbf{0})]$ ;
  end for
  if  $\min(w) \geq 2N + 2$  then
    for  $s$  in  $\mathbf{S}$  do
       $\mathbf{c} = \mathbf{C}s$ ;
       $\mathbf{W} = [\mathbf{W}|\mathbf{c}]$ ;
    end for
    if no repeat element in  $\mathbf{W}$  then
      return  $\mathbf{W}$ 
    end if
  end if
end while

```

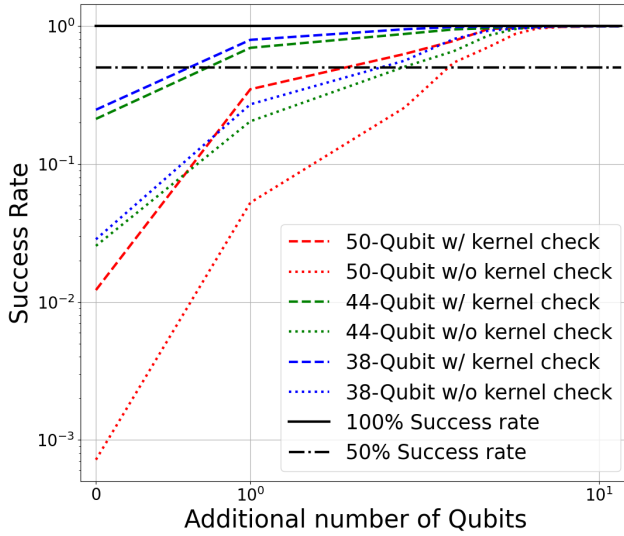


FIG. 4. This figure illustrates the impact on the success probability of generating \mathbf{G} when adding extra qubits to the generator. The x-axis shows the number of auxiliary qubits and the y-axis is the success rate. The dashed line, which resulted from a codeword check generated in Eqn~(G1), shows a systematic improvement in success rate compared to the unchecked (dotted line) case.

repetitions. This process is repeated until the minimum Q is found.

2. Scaling of RLE

We examine the scalability of RLE. The algorithm has a computation cost proportional to $\mathcal{O}(M^N)$ for each physical state check, multiplied by the number of checks performed. This complexity scaling is comparable to the Brouwer-Zimmermann algorithm, which is recognized as the most efficient method for checking the minimal distance of \mathbf{C} [45]. RLE also shares the same computational cost as non-linear encoding [12], but it is much simpler to implement. We can further enhance RLE scalability by incorporating auxiliary qubits into the optimal encoding. Figure 4 summarizes the success probability of generating the correct parity check matrix \mathbf{G} for 4-electron systems with auxiliary qubits. The algorithm's runtime exponentially converges to $\mathcal{O}(M^N)$ — the complexity for one check — when auxiliary qubits are successively added.

Appendix H: Fermionic Expectation Decoder

FED, as depicted in Algorithm 1, avoids direct fermionic operator representation through a decoding process. This approach circumvents the issue of measuring an unscalable number of Pauli operators and maintains polynomial scaling in measurement complexity. FED computes the expectation of the operator in Eqn~(D13), from which a probability distribution $P(\vec{d})$ is sampled in the basis $\vec{d} = (1/0_B, \vec{m}(\vec{b}))$. To decode the bitstrings from $\mathbf{G}\vec{b}$ to \vec{b} , reversing the Clifford transformation is necessary to retrieve the projector $\mathbf{G}\vec{b}$ from \vec{d} —a task that is infeasible for classical post-processing.

Instead, when computing the fermionic sign $(-1)^{\vec{b}\cdot\vec{c}}$, a partial recovery transformation can focus solely on recovering either $P^{\mathbf{G}\vec{b}}$ or $P^{\mathbf{G}(\vec{a}\oplus\vec{b})}$ as shown in Eqn~(5). Collectively, this is equivalent to retrieving the projector information $X^{\mathbf{G}\vec{a}}(P^{\mathbf{G}\vec{b}} + P^{\mathbf{G}(\vec{a}\oplus\vec{b})})$. This can be achieved through the CNOT transformation \hat{C} in Eqns~(D11) and (D12), which can be efficiently implemented on a classical computer directly on the bitstrings of the histogram as \mathbf{A} .

Under our operator decomposition, we avoid two problems that arise in non-linear encoding: firstly, we avoid preparing an exponential number of measurement bases; and secondly, we avoid calculating expectation values in the encoded space, which would decompose into an exponential number of Pauli strings. The projector representation in Eqn~(5) avoids the Pauli representation of the encoded operator under conserved subspace compression. This new representation establishes a direct link to the decoding protocol of the CEC code and classifies the complexity of measurement grouping within the conserved subspace. Overall, this leads to a scalable encoding and decoding process for simulating systems with conserved particle numbers.